coatings

MDPI

Review

Recent Progress in Electromagnetic Wave Absorption Coatings: From Design Principles to Applications

Yang Jin [1,2], Haojie Yu [1,2,*], Yun Wang [3], Li Wang [1,2,*] and Bohua Nan [4,*]

[1] State Key Laboratory of Chemical Engineering, College of Chemical and Biological Engineering, Zhejiang University, Hangzhou 310058, China; 3210100595@zju.edu.cn
[2] Zhejiang-Russia Joint Laboratory of Photo-Electro-Magnetic Functional Materials, College of Chemical and Biological Engineering, Zhejiang University, Hangzhou 310058, China
[3] Zhejiang Tuanyuan Composite Materials Co., Ltd., Pinghu 314200, China; yun.w@tuanyuanfc.com
[4] Shanghai Aerospace Equipments Manufacturer Co., Ltd., Shanghai 200240, China
* Correspondence: hjyu@zju.edu.cn (H.Y.); opl_wl@dial.zju.edu.cn (L.W.); nanbohua5@163.com (B.N.)

Abstract: It is essential to develop electromagnetic (EM) wave-absorbing materials with exceptional versatility to address a variety of applications, including anti-radar stealth, EM radiation protection, and EM interference shielding. EM wave absorption coatings, mainly composed of matrices and EM absorbers, have excellent practical performance. Researchers have been developing advanced EM absorption coating with properties like thin, light, broadband, and anti-aging. This review summarizes the recent progress in EM absorption coatings, including the design principles, feedstocks, manufacturing techniques, performance evaluation methods, and applications. Finally, the current challenges and future research directions are discussed.

Keywords: electromagnetic absorption materials; electromagnetic shielding; functional coatings

Citation: Jin, Y.; Yu, H.; Wang, Y.; Wang, L.; Nan, B. Recent Progress in Electromagnetic Wave Absorption Coatings: From Design Principles to Applications. *Coatings* **2024**, *14*, 607. https://doi.org/10.3390/coatings14050607

Academic Editors: Indrani Coondoo and Igor Bdikin

Received: 26 March 2024
Revised: 2 May 2024
Accepted: 9 May 2024
Published: 11 May 2024

1. Introduction

Electromagnetic (EM) absorption materials have garnered substantial research interest, particularly in the realm of military defense [1]. Aircraft with EM absorption bodies could be undetectable by radar and excel in covert operations [2]. Nowadays, EM absorption materials hold significant importance in civil applications [3,4]. This is due to the prevalence of EM technology in modern society, which includes medical imaging [5], wireless communication [6] and automobile navigation [7]. However, it is crucial to avoid exposing electric-powered facilities to excessive levels of EM radiation, as it can be detrimental to public health and potentially induce EM interference [8–10]. Pregnant women suffer from an increasing rate of abortions if exposed to EM fields above 16 mG or 50 Hz [11]. Strong EM fields are capable of disrupting a heart pacemaker [12,13], posing a threat to the patient. As a result, it is essential to develop EM-absorbing materials with exceptional versatility to accommodate various scenarios.

The practical performance of EM absorption coatings, which consist primarily of matrices and EM absorbers, is exceptional. As the dispersing medium for EM absorbers and other fillers, matrices facilitate substrate adhesion. EM absorption coatings apply to various substrates, including metal [14], plastic [15], textile [16], etc. The fundamental constituents of the coatings are EM absorbers, which perform the critical function of EM absorption. EM absorbers are conceptualized in accordance with an EM absorbing mechanism, which incorporates impedance matching [17,18], magnetic dissipation [19], dielectric dissipation [20] and multiple reflections [21]. The fundamental objective in designing EM absorbers is to manipulate the EM parameters through modifications in the structure and composition.

Traditional EM absorbers are magnetic materials such as ferrite [22] and dielectric materials like carbons [23]. They fail to achieve high EM dissipation or impedance matching

and easily lose EM absorption properties due to aging [24]. Recently, novel materials have been reported as promising EM absorbers, such as metallic nanomaterials [25–27], MXene composites [28–30] and Metal-Organic Framework (MOF) [31,32]. These newly designed absorbers feature refined nanostructures, which contribute to their improved EM absorption capabilities. Metallic nanomaterials have gained significant interest due to their distinct quantum size effect and electron structure. MXene composites, consisting mainly of early transition metal carbides and carbonitrides, show excellent dissipation performance and impedance matching. MOF possesses a molecular structure that can be modified, and the combination of ferromagnetic metal ions adds dielectric dissipation and magnetic properties to MOF.

A breakthrough in EM absorbers has been observed in recent years. Nevertheless, additional research is necessary to determine whether these absorbers are processable. Thermal spraying, liquid processing and vapor deposition are commonly used in the coating industry for the manufacturing of EM absorption coatings [33–35]. Different fabrication techniques have different applicability ranges for materials. EM absorption coatings must meet the requirements of these preparation techniques. Coatings for thermal spray have to be heat-resistant, and coatings for liquid processing must have good rheological properties.

This review aims to provide an overview of the recent progress in EM absorption coatings. A literature search was conducted to gather the studies on EM absorption coatings. We searched on Web of Science to find relevant articles published between 2015 and 2024, with keywords including "EM absorption coatings", " EM absorber", " EM absorbing mechanism", and similar terms. The review begins with the design principles of EM absorption coatings, followed by the introduction of feedstocks, fabrication techniques and performance evaluation methods. Finally, the current challenges and future research directions are discussed.

2. Design Principles of EM Absorption Coatings

EM absorption coatings are designed under the guidance of EM absorbing principles. However, some principles are still in dispute, such as quarter wavelength theory [36]. We present only the widely accepted principles in this section, including impedance matching, magnetic dissipation, dielectric dissipation and multiple reflections. According to these principles, EM parameters are the essential influencing factors to the absorption performance of the coating.

2.1. Impedance Matching

The widely used transmission line model represents single-layer homogeneous absorption coatings on a metal backing (Figure 1) [18,37]. The metal backing is treated as an ideal conductor with infinite conductivity. EM wave only penetrates its surface, resulting in complete reflection at the coating-metal backing interface. The metal backing is considered as a short-circuit load, represented by a load impedance of $Z_L = 0$. The propagation of EM wave occurs solely in the air and the coating, both acting as transmission lines. Unlike an ideal circuit, the EM wave dissipated while propagating through the air and the coating. The reflection loss (RL) of the circuit can be calculated by Equation (1) [18,37].

$$\mathrm{RL} = 20\ \log|(Z_{in} - Z_0)/(Z_{in} + Z_0)\ | \tag{1}$$

where Z_0 is the impedance of the free space and Z_{in} is the characteristic impedance related to the coatings. Z_{in} can be calculated by Equation (2).

$$Z_{in} = Z_0\sqrt{\frac{\mu_r}{\varepsilon_r}}\tanh\left\{j\left(\frac{2\pi f d}{c}\right)\sqrt{\mu_r\varepsilon_r}\right\} \tag{2}$$

where ε_r is the relative permittivity, μ_r is the relative permeability, d is the thickness of the coatings, f is the frequency of the incident EM waves and c the speed of light in vacuum. RL approaches infinite if $Z_{in} = Z_0$, and all the energy of the incident wave is dissipated.

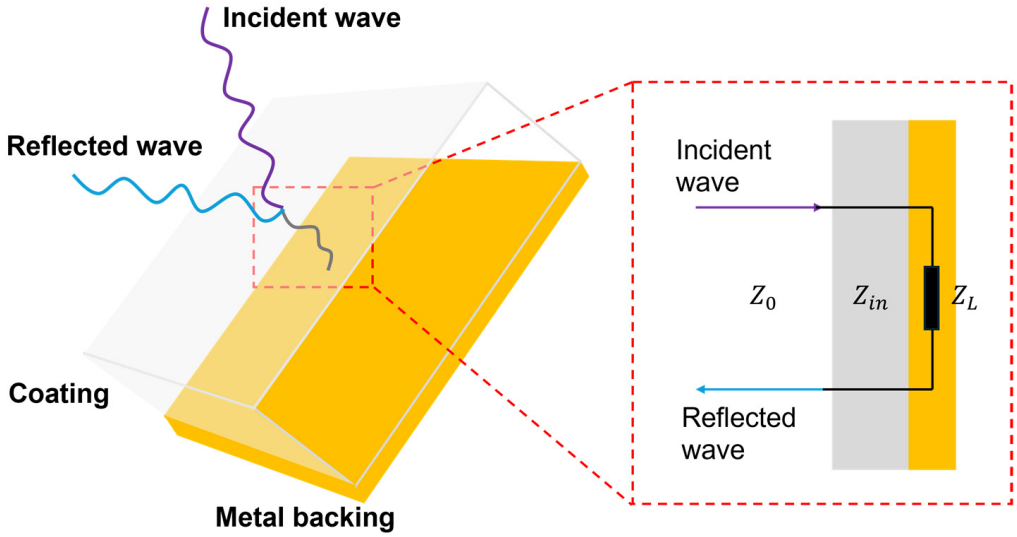

Figure 1. The transmission line model.

2.2. Magnetic Dissipation

Magnetic dissipation is caused by the magnetization and reverse magnetization of magnetic components in the coating, which is determined by the complex permeability. The relative permeability (μ_r) can be described by Equation (3), and the apparent magnetic dissipation is correlated to the tangent loss (Equation (4)) [38].

$$\mu_r = \mu' - j\mu'' \tag{3}$$

$$tan\delta_\mu = \frac{\mu''}{\mu'} \tag{4}$$

Magnetic dissipation can be further divided into three parts, including hysteresis loss, eddy current loss and residual loss. The energy dissipated at a given frequency (f) can be expressed by Equation (5) [19].

$$W(f) = W_h + W_{eddy}(f) + W_r(f) \tag{5}$$

where W_h is the hysteresis loss, $W_{eddy}(f)$ is the eddy current loss and $W_r(f)$ is the residual loss. The hysteresis loss is caused by the movement of the domain wall and the rotation of the magnetic moment [37]. Therefore, W_h relies solely on the magnetic properties of the coatings, and is independent of the frequency of the EM wave. The eddy current is induced by the alternative EM field and dissipates the EM energy as well. Residual loss includes other kinds of magnetic dissipation, such as magnetic aftereffects and resonance.

2.3. Dielectric Dissipation

The EM wave is dissipated in dielectric materials through conductive loss and polarization loss. The dielectric dissipation of the coating is determined by the complex permittivity. The relative permittivity (ε_r) can be described by Equation (6), and the apparent dielectric dissipation is correlated to the tangent loss (Equation (7)) [39].

$$\varepsilon_r = \varepsilon' - j\varepsilon'' \tag{6}$$

$$tan\delta_\varepsilon = \frac{\varepsilon''}{\varepsilon'} \tag{7}$$

where ε' is the real part of permittivity and ε'' is the imaginary part of permittivity. From Equation (7) it is noticed that dielectric dissipation is correlated to ε'', which can be further described as Equation (8) [20].

$$\varepsilon'' = \varepsilon_c'' + \varepsilon_p'' \tag{8}$$

where ε_c'' is correlated to the conductive loss and ε_p'' is correlated to the polarization loss. ε_c'' is proportional to the electrical conductivity (σ), because when the EM wave propagates in conductive materials, electric current is induced and the EM energy is dissipated as Joule heat. Polarization loss can be further divided into interfacial polarization, dipolar polarization, and defect-induced polarization [40]. Interfacial polarization is associated with the interface of phases with different permittivity. Dipolar polarization is caused by the displacement polarization of nonpolar molecules and the orientation polarization of polar molecules in the EM field. Defect-induced polarization is related to defect sites such as vacancies and doping atoms.

2.4. Multiple Reflections

Multiple reflections occur if the coating is thin enough (Figure 2). A portion of the EM wave that has passed through the front interface reflects from the back interface and travels towards the front interface. Through the reflection process, the energy of the EM wave is dissipated. However, the dissipation becomes negligible when the thickness of the coating exceeds the skin depth, which is the distance below the surface of a shield where the intensity of the EM field decreases to $1/e$ (≈ 0.368) of its initial value. The skin depth (δ) can be calculated by Equation (9) [21].

$$\delta = \frac{1}{\sqrt{\pi f \sigma \mu}} \tag{9}$$

where σ is the conductivity of the coating and μ is the permeability. However, if the coating is thinner than the skin depth, EM waves can travel between the front and back interfaces without significant dissipation.

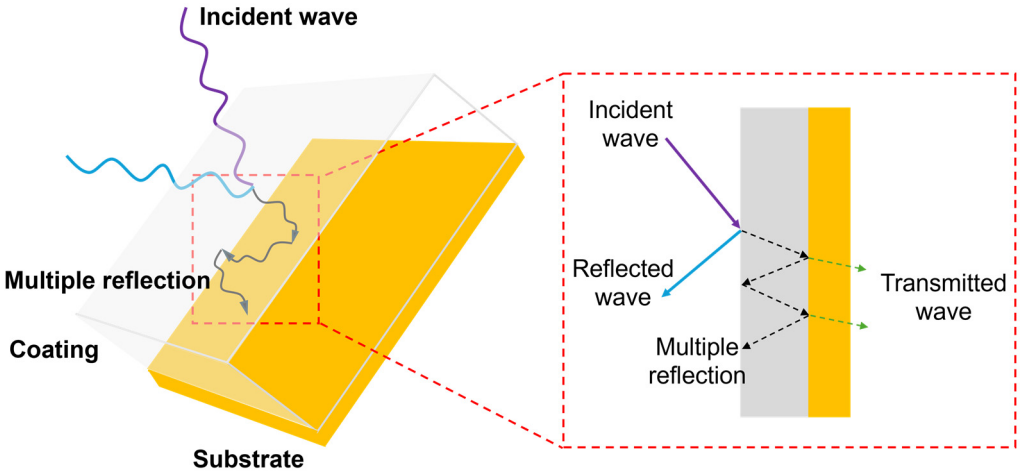

Figure 2. The multiple reflection of EM waves in the coating.

3. Feedstocks of EM Absorption Coatings

Feedstocks of EM absorption coatings mainly consist of matrices and EM absorbers. Examples of commonly used matrices are briefly introduced. Various kinds of EM absorbers are discussed in detail based on their EM absorption mechanisms.

3.1. Matrices

3.1.1. Polymer Matrices

Polymers, usually with excellent mechanical properties and low permeability, are conventional matrices for EM absorption coatings [41]. Epoxy resin has been the most famous polymer matrices because of its excellent processibility and adhesivity. Epoxy resin can be blended with EM absorbers in any proportion and avoid their agglomeration during the manufacturing process. The epoxy groups of the resin guarantee strong adhesion between the coating and the substrate. Besides, polymers such as polypropylene (PP) [42], polyurethane (PU) [43] and acrylic resin [44] are promising matrices as well. These polymer matrices are durable at room temperature but cannot withstand heat and oxidation in harsh environments.

3.1.2. Ceramic Matrices

The ceramic is the most widely studied inorganic matrix for EM absorption coatings [45]. Compared with organic matrices, the ceramic is anti-oxidative and heat-resistant. Therefore, the ceramic is promising for high-temperature EM absorption. EM parameters such as permittivity (Figure 3) should be considered when choosing the right kind of ceramic matrix. Dielectric ceramics with relatively high permeability absorb EM waves by dielectric dissipation. Thus, dielectric ceramics can be used directly as EM absorption coatings. Ceramics with low permeability like Al_2O_3 and SiO_2 are EM transparent. These low-permeability ceramics are ideal matrices for EM absorbers.

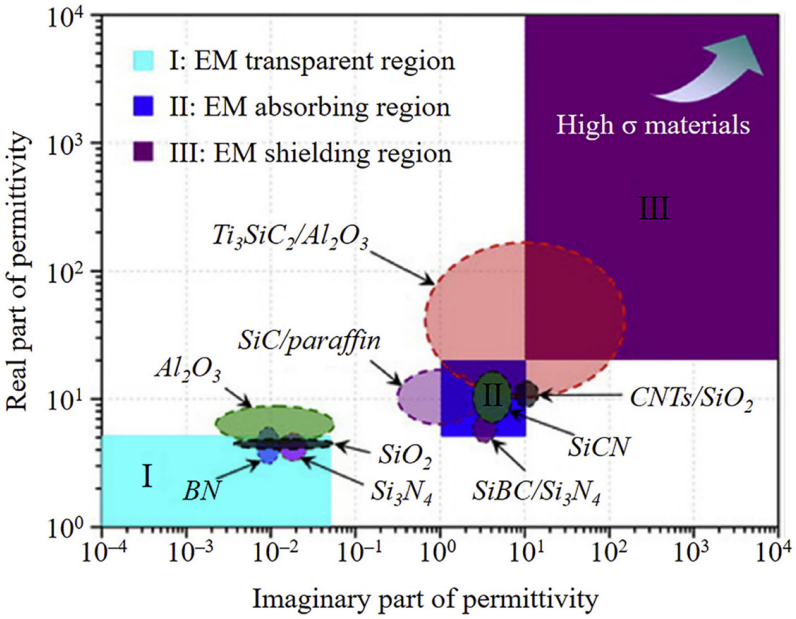

Figure 3. The relative permittivity of typical dielectric ceramics. Reprinted with permission from [45].

3.2. EM Absorbers

The absorption properties of the coating primarily depend on EM absorbers. In this section, we discuss four kinds of EM absorbers, including carbon materials, metallic composites, ferromagnetic materials and metamaterials. Their dissipation performance and typical operating frequencies are listed in Table 1. It is noticed that dielectric dissipation is more common than magnetic dissipation in all kinds of EM absorbers, except ferromagnetic materials. Perhaps that is because dielectric properties such as conductivity are easier to tailor than magnetic properties.

Table 1. The tangent loss and typical operating frequencies of EM absorbers.

Kind of Absorbers	Name	$tan\delta_\varepsilon$ *	$tan\delta_\mu$ **	Dominate Dissipation Mechanism	Typical Operating Frequencies (GHz) ***	RL_{min} (dB)	Reference
carbon materials	Fe/C hollow sphere	0.50~1.00	≈0.05	dielectric	6~18	−62.7	[46]
	N-CNTs encapsulated Co/Ni	0.05~0.55	−0.1~0.1	dielectric	6~10	−84.0	[47]
	Ag@SG	0.27~0.325	/	dielectric	9~12	−15	[48]
metallic composites	Ni-SAs/NC	0.20~0.60	≈0.0	dielectric	8~14	−36.4	[27]
	Co_{1+Cs}/NGC	0.30~0.75	≈0.0	dielectric	10~18	−54.3	[26]
	MXene/polyaniline	0.2~1.2	0.0~0.4	dielectric	5~11	−60.6	[49]
	NiCoFe@C	≈0.33	0.07~0.15	dielectric and magnetic	9~11	−47.6	[50]
	$Ni/Ni_3ZnC_{0.3}$	0.5~1.5	0.05~0.2	dielectric and magnetic	12~18	−56.8	[51]
	Zn-HHTP	0.16~0.23	/	dielectric	2~10	−62.8	[52]
	MOF@MOF	0.20~0.95	−0.3~0.3	dielectric	10~18	−40	[53]
ferromagnetic materials	RGO@FGT	0.4~1.0	−0.2~0.15	dielectric and magnetic	11~14	−61	[54]
	P[AVIm][$HoCl_4$]/rGO	0.2~0.35	0.05~0.25	magnetic	10.5−15.6	−57.32	[55]
metamaterials	gyroid structured carbon-based material	/	/	dielectric	2~40	−40	[56]
	TPMS-Shellular structured SiOC ceramics	0.41~0.56	/	dielectric	12~18	−72.38	[57]

* The data were estimated from $tan\delta_\varepsilon$-frequency plot or ε_r-frequency plot. ** The data were estimated from $tan\delta_\mu$-frequency plot or μ_r-frequency plot. *** The operating frequencies were estimated from the RL-thickness-frequency graph.

3.2.1. Carbon Materials

Carbon materials are one of the most outstanding EM absorbers. Their EM absorption properties are mainly caused by dielectric dissipation, but magnetic dissipation works as well if they are doped with metals (Figure 4) [58,59]. Carbon materials are lightweight and anti-corrosion. However, impedance mismatch limits their absorption performance [60]. Compositing carbon materials with magnetic materials is a popular solution. Many EM absorbers are carbon composite materials, such as metallic nanomaterials and MOF derivatives. These materials are discussed in other sections. In this part, we discuss three kinds of carbon materials, including carbon nanoparticles (CNPs), carbon nanotubes (CNTs) and graphene.

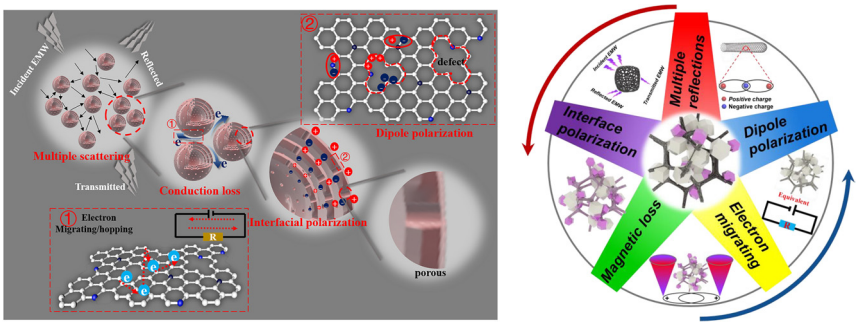

Figure 4. Possible EM absorption mechanisms of carbon materials. Reprinted with permission from [58,59].

Wu et al. reported the gradient-structured Fe/C nanosphere with strong RL and improved impedance matching [46]. In their preparation process, the ferrocene disinte-

grated into iron oxide and cyclopentadiene. at the same time, iron oxide competed with the polycyclopentadiene to grow on the crystal nucleus. Therefore, the gradient anchor of iron oxide in the polycyclopentadiene was formed. After etching and pyrolysis, the nanosphere exhibited a hollow structure with more Fe near the core and less Fe on the shell (Figure 5a). The nanosphere showed a reflection loss (RL) of −62.7 dB at the thickness of 2.1 mm. Zhang et al. optimized the impedance matching of N-doped CNTs (N-CNTs) by encapsulating Co/Ni alloy (Figure 5b) [47]. N-CNTs/Co/Ni nanocomposite exhibited a $|Z_{in}/Z_0|$ value closer to 1, indicating its excellent impedance matching properties. Liu et al. prepared the Ag-decorated spherical graphene (Ag@SG) and blended it with PU resin (Figure 5c) [48]. After being decorated with Ag the impedance of SG approached that of the free space, which was close to the ideal condition of impedance matching.

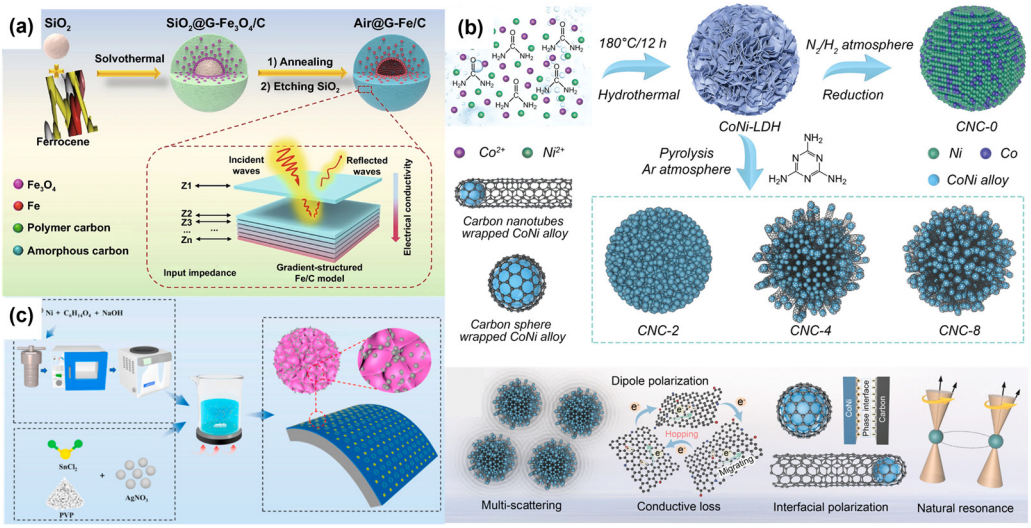

Figure 5. Scheme of (**a**) the preparation of gradient-structured Fe/C nanosphere [46], (**b**) the preparation and EM absorption mechanism of N-CNTs encapsulated Co/Ni [47], and (**c**) the preparation of Ag@SG [48]. Reprinted with permission from [46–48].

3.2.2. Metallic Composites

Metallic composites like metallic nanomaterials, MXenes, and MOFs have gained considerable attention in the recent development of EM absorbers. They can be engineered with desired electromagnetic properties by adjusting the composition and structure. Metallic composites can achieve broadband absorption of EM waves, but the complex preparation method limits their application.

Metallic Nanomaterials

Metallic nanomaterials have garnered substantial research interest, because of their distinct quantum size effect and electron structure. Recently, researchers have been developing metallic single atoms (SAs) as the EM absorber. The EM properties of SAs are better than the corresponding nanoparticles (NPs). That is because every isolated metal atom forms a polarization center. The polarization centers increase the dielectric dissipation of SAs (Figure 6) [25].

Liang et al. fabricated Ni single-atom sites/N-doped carbon (Ni-SAs/NC) by ligand polymerization (Figure 7) [27]. The ligand strategy involved attaching ligand sites to support groups. Chitosan captured and anchored Ni precursors by amino and hydroxyl groups. Ni in Ni-NPs was zero-valent, but Ni in Ni-SAs/NC was $Ni^{\delta+}$ ($0 < \delta < 2$). The cation $Ni^{\delta+}$ possessed a higher density of unpaired 3d electrons that enhanced the polarization dissipation. Ni-SAs/NC showed an effective absorption bandwidth (EAB) of 7.08 GHz at the thickness of 2.50 mm, which was much better than Ni-NPs/NC. Liu et al. reported an EM absorber composed of Co-SAs and Co-cluster on nitrogen-doped graphitic carbon

(Co_{1+Cs}/NGC) [26]. The composite exhibited an EAB of 7.0 GHz at the thickness of 2.0 mm. When the number of Co atoms reached a certain amount, Co–Co bonds were formed according to density functional theory. The large circular dipoles were generated and improved the dipolar polarization of NGC. However, if the concentration of Co increased to 7.0 wt%, Co atoms would agglomerate into zero-valence Co-NPs. The formation of Co-NPs weakened the polarization dissipation.

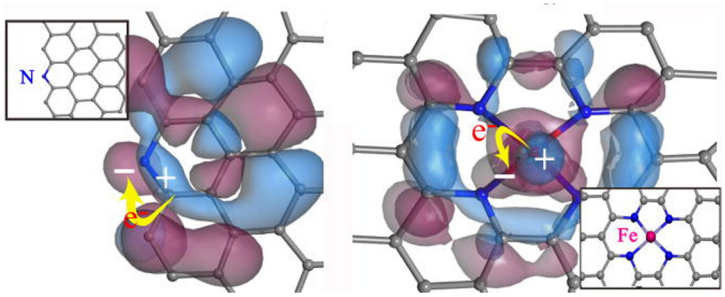

Figure 6. The EM absorption mechanisms of transition metal SAs. Reprinted with permission from [25].

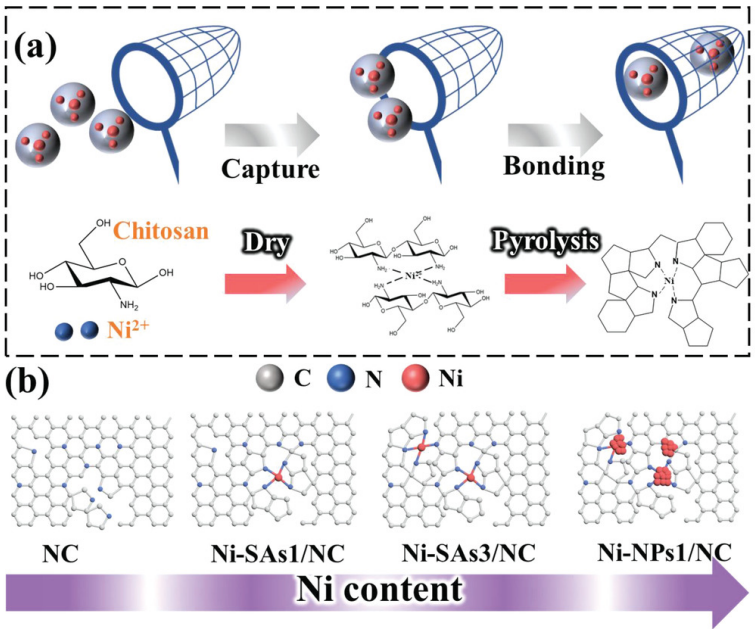

Figure 7. Scheme of (**a**) the preparation of Ni-SAs/NC and (**b**) the structure of NC, Ni-SAs/NC and Ni-SAs/NC. Reprinted with permission from [27].

MXenes

MXenes are a group of two-dimensional materials consisting of early transition metal carbides and carbonitrides [61]. These 2D materials are promising EM absorbers because of their high conductivity, permittivity and interfacial defects [62], which contributes to dielectric dissipation (Figure 8) [63].

High permittivity may lead to impedance mismatch, which decreases the EM absorbing performance of MXenes [64]. Thus, MXene has been prepared into composites with better impedance matching. Zhang et al. prepared $Ti_3C_2T_x$ hollow spheres by sacrificial template method (Figure 9a) [65]. The hollow structure enlarged the inter-sheet space and increased the interfacial polarization between the 2D absorbers and the air. Zhou et al. fabricated $Ti_3C_2T_x$/PEO aerogels by ice-templated lyophilization [64]. The air filling in the aerogels had the same impedance as the free space. Therefore, the impedance matching of $Ti_3C_2T_x$/PEO was improved. Yu et al. prepared MXene/polyaniline composition by

in situ polymerization (Figure 9b) [49]. With the increasing content of polyaniline in the composite, the permittivity (ε) of the composition decreased. The decreasing permittivity improved the impedance matching.

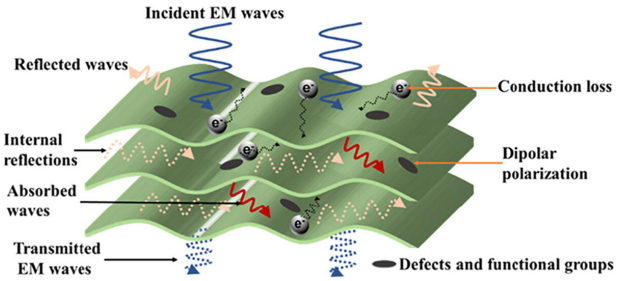

Figure 8. Possible EM absorption mechanisms of MXenes. Reprinted with permission from [63].

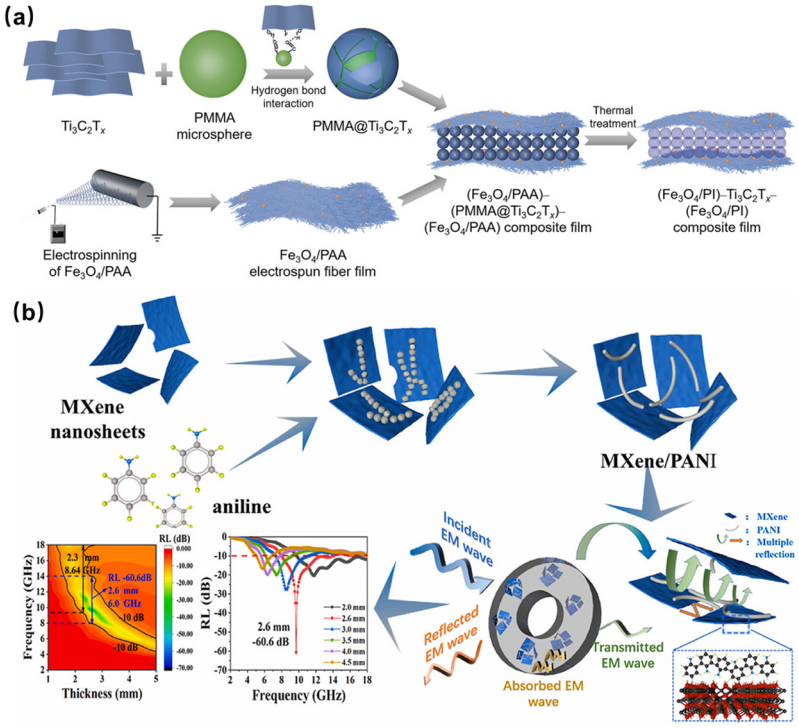

Figure 9. The preparation of (**a**) Fe_3O_4/polyimide/$Ti_3C_2T_x$ [65] and (**b**) MXene/polyaniline [49]. Reprinted with permission from [49,65].

MOF and Its Derivatives

MOF is a large family of compounds consisting of metal ions and organic ligands. The tunable molecular scaffold of MOF allows the customization of its EM properties. Various EM dissipation mechanisms have been applied to fabricate EM absorbers from MOF (Figure 10) [21].

Zheng et al. prepared a series of core–shell structured Prussian blue analog (PBA) derivatives, namely NiFe@C, CoFe@C, NiCo@C, and NiCoFe@C [50]. Among them, NiCoFe@C exhibited the lowest RL of −47.6 dB at 1.7 mm. The improved RL was due to the coupling effect of magnetic alloys. Xie et al. prepared an anti-corrosion EM absorber of $Ni/Ni_3ZnC_{0.3}$ [51]. $Ni/Ni_3ZnC_{0.3}$ was prepared by the pyrolysis of NiZn-MOFs. The carbon shell wrapping around $Ni/Ni_3ZnC_{0.7}$ particles increased the number of defect sites and served as a barrier against corrosion. $Ni/Ni_3ZnC_{0.7}$ exhibited a RL of −56.8 dB at the thickness of 2.40 mm. The MOF remained stable after being immersed in corrosive mediums for 6 months.

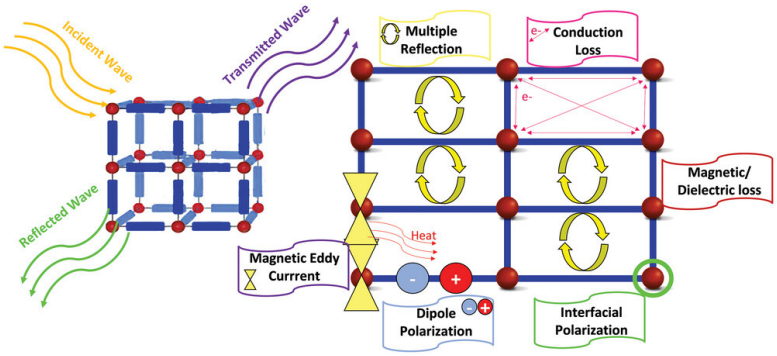

Figure 10. Possible EM absorption mechanisms of MOF and its derivatives. Reprinted with permission from [21].

Researchers have been developing raw MOFs for EM-absorption as well because the pyrolysis of MOF was energy-consuming. Zhang et al. reported the EM absorption properties of raw MOFs with metal ions such as Zn, Cu, Co, or Ni and hexahydroxytriphenylene (HHTP) ligands (Figure 11a,b) [52]. Among the MOFs prepared by different types of metal precursors, Zn-HHTP demonstrated the highest permittivity and largest aspect ratio. The shape anisotropy induced single-crystal volume polarization and thus increased the dielectric dissipation. Liu et al. designed the "Matryoshka Doll" structured MOF@MOF (Figure 11c,d) of two different Zeolitic Imidazolate Frameworks (ZIF), namely ZIF-67 and ZIF-8 [53]. The multilayer MOF possessed abundant heterogeneous interfaces and defect sites which increased the dielectric dissipation. The five-layer MOF exhibited an EAB of 4.4 GHz at the thickness of 1.56 mm.

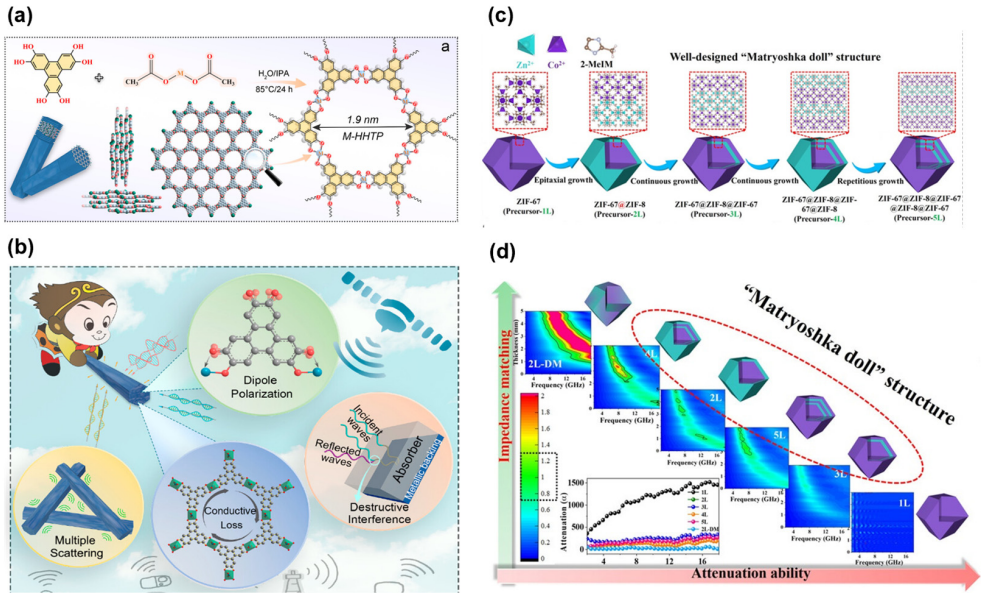

Figure 11. Scheme of (**a**) the structure of the HHTP derived MOFs, (**b**) the EM absorption mechanism of HHTP derived MOFs, (**c**) the structure of MOF@MOF and (**d**) the EM absorption mechanism of MOF@MOF. Reprinted with permission from [52,53].

3.2.3. Ferromagnetic Materials

Ferromagnetic materials, such as ferrites and metal alloys, absorb EM waves by magnetic dissipation (Figure 12) [60]. Ferromagnetic materials have a strong magnetic response to the EM field, which ensures excellent absorption properties. However, their application is limited by the low Curie temperature (Tc), at which materials transit to a disordered state and lose EM absorption properties [54]. Therefore, researchers have

been developing heat-resistance ferromagnetic absorbers with high Tc. Niu et al. prepared the $LaFe_{12}O_{19}$ ceramic by air plasma spray coating [66]. The ceramic coating exhibited a RL of −39.30 dB at the thickness of 4.5 mm and remained stable after heat treatment at 1000 °C. Li et al. prepared a reduced graphene oxide@Fe_3GeTe_2/$FeTe_2$/Fe_3Ge (RGO@FGT) foam [54]. The foam was prepared by the annealing treatment of graphene oxide@Fe_3GeTe_2. During the annealing, Fe_3GeTe_2 partially decomposed into $FeTe_2$ and ferromagnetic Fe_3Ge. Fe_3Ge has a Tc of 623 K, and the foam achieved a Tc of 496 K. The magnetic coupling of Fe_3Ge and Fe_3GeTe_2 maintained the ferromagnetic order at high temperatures and thus increased the Tc. Xia et al. prepared an EM absorbing film of poly(1-allyl-3-vinylimidazolium)[$HoCl_4$]/RGO (P[AVIm][HoCl4]/rGO) [55]. The film showed Tc ≈ 486 K and was the first ferromagnetic polymer composite at room temperature. The π–π stacking between the imidazole ring and the graphene ring anchored the imidazole cation polymer. The magnetic moment between imidazole cation and $[HoCl_4]^-$ was restricted. The restricted magnetic moment formed magnetic domains, and thus the polymer was ferromagnetic.

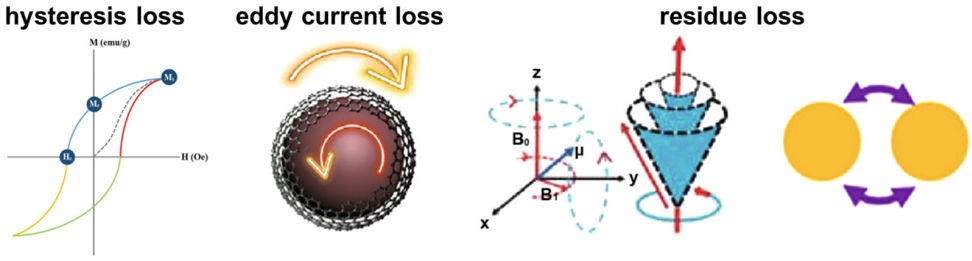

Figure 12. Possible EM absorption mechanisms of ferromagnetic materials. Reprinted with permission from [67,68].

3.2.4. Metamaterials

Materials with array structure at the subwavelength scale are named metamaterials [69]. Metamaterials show unexpected EM properties than bulk materials of the same composition. The meta-structure enhances the EM interference and conductive loss within the material and improves the EM absorption properties (Figure 13) [56]. Therefore, metamaterials can be designed into EM absorbers. An et al. fabricated a gyroid-structured acrylonitrile butadiene styrene plastic (ABS) by 3D printing [56]. The meta-structure plastic was then coated with carbon-based dielectric materials. The metamaterial showed RL ≤ −10 dB across a wide band range (2–40 GHz). Yao et al. fabricated a SiOC ceramic-based metamaterial with high-temperature EM absorption properties [57]. The material was of triply periodic minimal surfaces (TPMS) and shellular structure. The TPMS-shellular structured metamaterial had an EAB of 5.60 GHz even at 600 °C. Metamaterials are designed based on mathematical theories and simulation to achieve perfect EM absorption properties. The top-down design methodology is better than other preparation method, which needs trial and error. However, the fabrication of metamaterial involves 3D printing technology, which has not yet been available for large-scale manufacturing of coating.

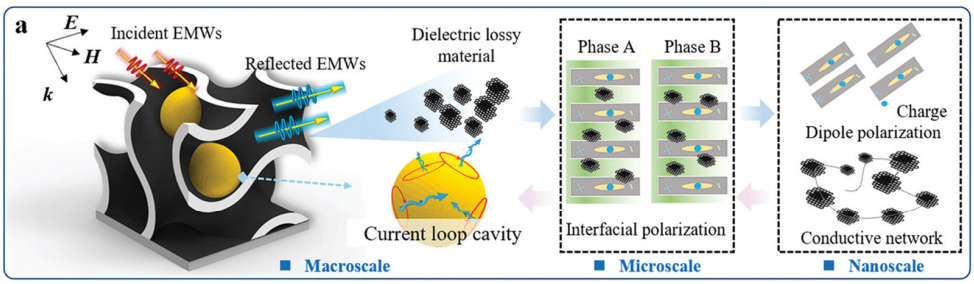

Figure 13. Possible EM absorption mechanisms of ferromagnetic materials. Reprinted with permission from [56].

4. Fabrication Techniques of EM Absorption Coatings

Thermal spraying, liquid processing and vapor deposition are common methods for the fabrication of EM absorption coatings. Thermal spraying involves the deposition of molten particles onto a substrate. Liquid processing techniques, such as blade coating and screen-printing, rely on the application of the liquid solution or suspension. Vapor deposition utilizes the evaporation of the precursor material and the deposition of it on the substrate. Each technique has its characteristics which are listed in Table 2.

Table 2. The characteristics of different fabrication techniques.

Fabrication Techniques	Advantages	Limitations	Suitability for Specific Material Types	Reference
thermal spray coating	versatile; rapid; reparable	high temperatures may damage EM absorbers	heat-resistant materials	[33,66]
liquid processing coating	low-cost; convenient	material wasting	soluble materials or materials that are dispersible in liquid	[34]
vapor deposition coating	excellent durability; precisely controllable	slow growth rate of coatings	materials with volatilizable precursors	[35]

4.1. Thermal Spraying Coating

Thermal spray coating technology, including cold spray, warm spray, flame spray, etc., has been widely used for preparing inorganic coatings [33]. In the thermal spray process, the feedstock is melted and sprayed onto the substrate (Figure 14). Air plasma spraying (APS) technology is one of the most famous thermal spraying technologies that utilizes plasma arc as the heat source [70]. The temperature at the center of the plasma arc reaches tens of thousands of degrees Celsius, which makes it possible to melt nearly any material. In the coating process, the feedstock powders are introduced into the plasma jet, melted and swiftly deposited onto the substrate [66]. APS offers advantages such as simplicity, rapid spraying speed and high powder deposition rate. However, the extremely high temperatures of the plasma flames may cause structural damage to EM absorbers, resulting in a decrease in absorption performance or even complete loss.

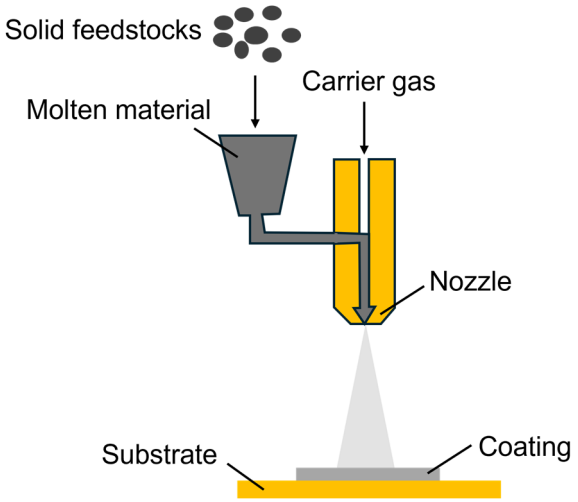

Figure 14. Scheme of thermal spray coating.

Utilizing heat-resistant ceramics can address the problem. Huang et al. prepared $Ba_4Fe_{2.6}Dy_{1.4}Nb_8O_{30}$ powder by solid-state reaction at 1300 °C [71]. The powder was mixed and milled with FeSiAl. The mixture was granulated and coated onto titanium and graphite substrate by APS. The composite ceramic powder exhibited remarkable phase

stability during APS. The coatings showed a RL of −48.20 dB at the thickness of 3.5 mm. Yao prepared B_4C/Al_2O_3 coating via ball milling, spray drying and APS [70]. The coating demonstrated a minimum RL of −39.58 dB and retained an effective absorption bandwidth of 1 GHz after annealing. A new idea of utilizing APS is to conduct chemical reactions in plasma flame. Ceramic coatings containing $LaFe_{12}O_{19}$ were fabricated by the chemical reaction between Fe_2O_3 and $LaFeO_3$ (Equation (10)) during APS [66]. At high-temperature O_2 was rapidly consumed, pushing the reaction rightward.

$$LaFeO_3 + \frac{11}{2}Fe_2O_3 \rightarrow LaFe_{12}O_{19} + \frac{1}{4}O_2 \quad (10)$$

4.2. Liquid Processing Coating

Liquid processing coating involves the liquid as the medium for the EM absorbers. For specific methods such as dip-coating, blade coating and screen-printing, the details are slightly different, but all of them follow a similar route (Figure 15). Firstly, the feedstock is dispersed into a liquid medium to prepare a solution or a suspension. Then, the liquid is applied to the substrate by dipping or scraping. Finally, the solvent is evaporated and dry coatings are formed on the substrate. Liquid processing coating is a low-cost and convenient way to prepare EM absorption coatings, but it is not suitable for bulk EM absorbers that are difficult to disperse in liquid. It is also notable that a large portion of feedstock is not coated on the substrate, which is a waste of material.

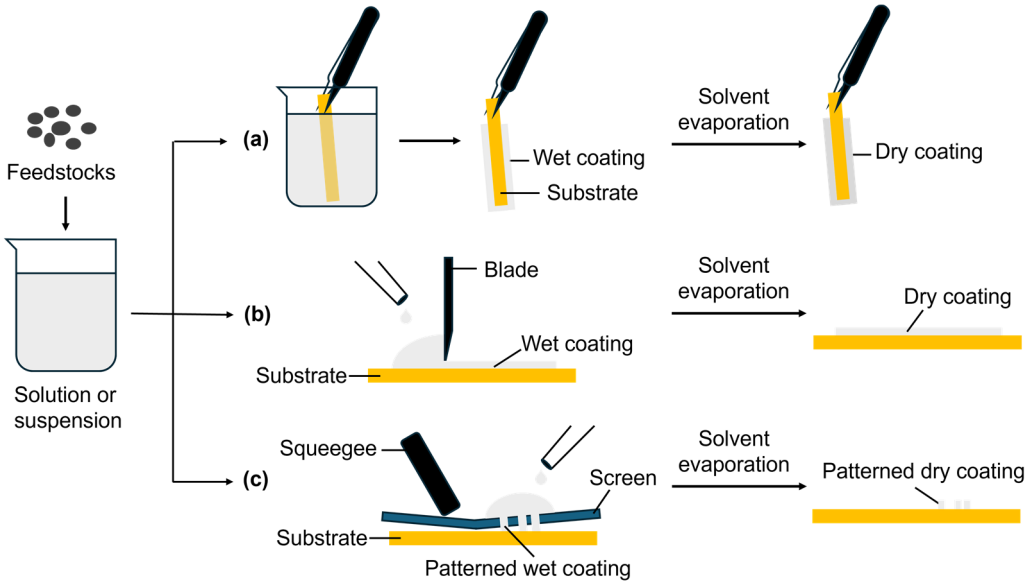

Figure 15. Diagrams for the process of (**a**) dip-coating, (**b**) blade coating and (**c**) screen printing.

To improve the processibility of the solution or the suspension, the rheological properties have to be regulated. Deng et al. reported catecholamines micro-crosslink MXene with enhanced viscosity and modulus [34]. Catecholamines such as dopamine (DA) with positively charged amino groups had a strong electro-statistic interaction with the negatively charged termination groups on MXene. The MXene ink with 0.5 wt% DA (m_{DA}:m_{MXene} = 0.5 wt%) showed a high viscosity of 180.4 Pa • s and an elastic (G′) and viscous (G″) moduli ratio of G′/G″ = 10. However, coagulation was discovered when directly mixing MXene with dopamine, because of the strong interaction between them. Deng et al. prepared polydopamine-graft-MXene (p-MXene) ink with tunable viscosity [72]. The amount of amino groups in poly-DA was less than that of DA, so the coagulation was avoided. The p-MXene was dispersed in water to prepare the ink. As the solid content increased, the viscosity of the ink increased as well. The highly viscous p-MXene ink with

60 mg/mL solid content was suitable for screen-printing, and the low-viscosity p-MXene with a solid content of about 10 mg/mL ink was capable of dip-coating.

Novel liquid processing coating technologies were reported for preparing nanocomposite coatings, such as vacuum-assisted filtration. The coating process applies a pressure differential across a filter medium. The liquid passes through the filter while the solid is retained in the medium. Ma et al. reported the Ag nanowire (AgNW) decorated sheep leather with excellent EM interference shielding properties [73]. The AgNW dispersion was filtered through the leather, and the AgNW intertwined with the collagen fiber bundles, thus constructing a 3D conductive network for EM dissipation.

4.3. Vapor Deposition Coating Technology

Vapor deposition involves the deposition of thin coatings onto a substrate (Figure 16). It begins by heating the precursor material, causing it to evaporate and form a vapor phase. The vapor is then directed towards the substrate, where it condenses and forms a thin coating. Vapor deposition offers advantages such as excellent durability. It also allows for precise control over the thickness and composition of the deposited coatings, enabling customization of the EM absorption coatings to optimize their performance. However, the deposition rate of the coatings is slow, and the thickness of the coating is usually within the order of μm [35].

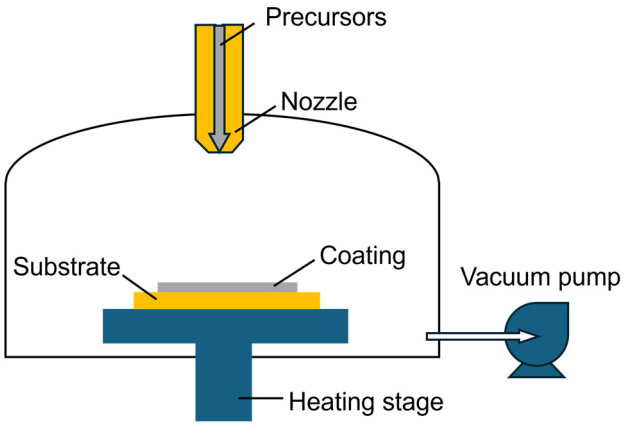

Figure 16. A diagram of vapor deposition coating.

Wang et al. prepared polypyrrole coatings on a polyamide (PA) mat via vapor deposition polymerization [74]. Polypyrrole was uniformly integrated with PA. The coated mat showed low reflection and high adsorption over a wide frequency range (8.2−12.4 GHz). Xie et al. fabricated the graphene coatings on quartz fiber (QF) by modulation-doped chemical vapor deposition (CVD) [35]. A roll-to-roll CVD system was designed for industrial implementation, which offered control over the rolling speed from 0.05 to 0.2 m/min^{-1}. The coated QF was 10 m long and showed excellent absorption properties across a wide frequency range (1–18 GHz).

5. Performance Evaluation of EM Absorption Coatings

EM absorption coatings are usually characterized mainly by their EM absorption performance, absorption mechanism and anti-aging performance. The performance evaluation methods and instruments are briefly introduced.

5.1. Measurement of Absorption Properties

The EM absorption properties of the coating can be characterized by the reflection and transmission of the incident wave, which is usually measured by the coaxial method and the arch method [75,76].

The coaxial method (Figure 17b) [75] is commonly used to measure the absorption properties of EM absorbers. It utilizes the vector network analyzer (VNA) (Figure 17a)

that measures the scattering parameters (S-parameters). S-parameters can be used to calculate the reflectivity or the trans reflectivity (R) and transmissivity (R) of the sample by Equations (11) and (12) [77].

$$R = \left|\frac{E_r}{E_i}\right|^2 = |S_{11}|^2 = |S_{22}|^2 \quad (11)$$

$$T = \left|\frac{E_t}{E_i}\right|^2 = |S_{21}|^2 = |S_{12}|^2 \quad (12)$$

where E_i is the intensity of the incident wave, E_r is the intensity of the reflected wave, and E_t is the intensity of the transmitted wave; S_{11}, S_{22}, S_{21} and S_{12} are S-parameters. The permittivity and permeability can also be determined by S-parameters according to the Nicolson–Ross–Weir method. Details for the correlation equation and derivation processes are complex, which can be found in the reference [78].

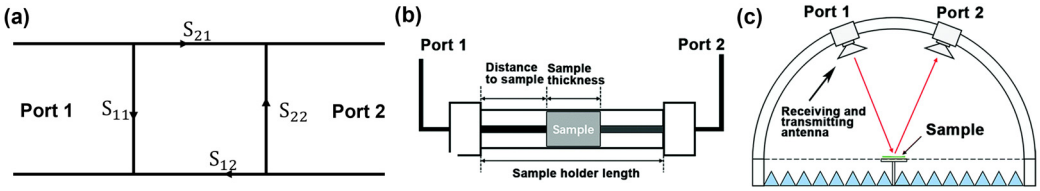

Figure 17. Diagrams of (**a**) the vector network, (**b**) instruments of the coaxial method and (**c**) instruments of the arch method. Reprinted with permission from [75].

For the coaxial method, EM absorbers must be prepared into the standard-sized sample. The EM absorber is mixed with paraffin or wax. The mixture is molded to prepare a sample for the measurement. This method is suitable for powder-like and granular absorbers. However, it is unsuitable for films or coatings on the substrate.

For large-scale coatings, the EM absorption properties can be measured by the arch method (Figure 17c) [75]. The arch method is conducted in a microwave anechoic chamber. Two antennas are placed at the top, and the sample is placed on a metal platform. The EM wave is emitted from one port (port 1), and the reflected wave is received by another port. The signal from both ports was analyzed by a scalar network analyzer, and the reflectivity (R) can be calculated by Equation (13) [79].

$$R = 10\log\left(\frac{P_a}{P_m}\right) \quad (13)$$

where P_a is the reflecting power of the sample and P_m is to the reflecting power of the metal plate.

5.2. Measurement of Dielectric Dissipation

According to the Debye theory, the EM absorption coating undergoes polarization relaxation if the permittivity is subject to Equation (14) [19].

$$\left(\varepsilon' - \frac{\varepsilon_s + \varepsilon_\infty}{2}\right)^2 + (\varepsilon'')^2 = \left(\frac{\varepsilon_s - \varepsilon_\infty}{2}\right)^2 \quad (14)$$

where ε_s is the statistic permittivity and ε_∞ is the permittivity at infinite frequency. Every semicircle on the $\varepsilon'' - \varepsilon'$ curve represents a polarization dissipation process. The semicircle on the curve is called the Cole-Cole semicircle. Complex permittivity at different frequencies can be measured by VNA, and the $\varepsilon'' - \varepsilon'$ curve can be plotted to analyze the polarization behavior of the coating (Figure 18) [20].

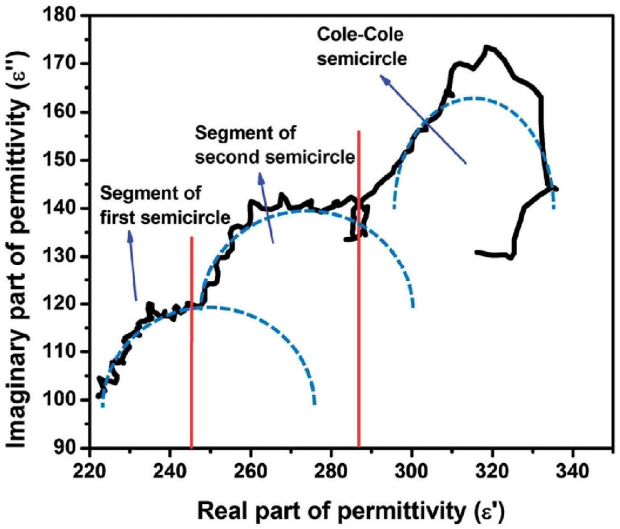

Figure 18. An example of the Cole-Cole plot. Reprinted with permission from [20].

5.3. Measurement of Hysteresis Dissipation

The magnetic hysteresis loops evaluate the hysteresis loss of the coating [80–82]. They can be measured by the vibrating sample magnetometer. In a hysteresis loop (Figure 19) [68], the saturation magnetization (M_s) refers to the maximum magnetization of the sample, and the remanent magnetization (M_r) refers to the magnetization in the sample after the external magnetic field disappears. The coercive force (H_c) is the amount of magnetic field that is applied to counteract the magnetization of the sample. M_s, M_r and H_c are all positively related to the magnetic dissipation of EM energy in the sample.

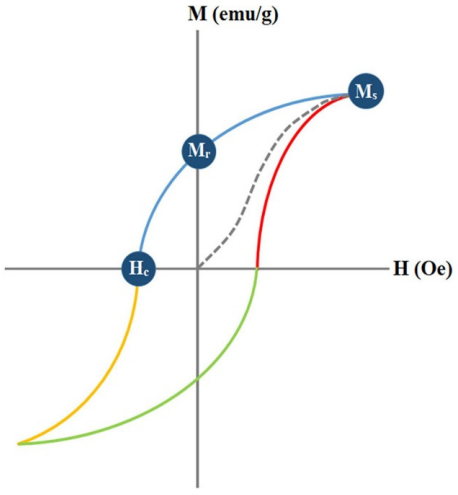

Figure 19. The M_s, M_r and H_c in a hysteresis loop. Reprinted with permission from [68].

5.4. Evaluation of Aging Resistance Performance

EM absorption coatings suffer from aging in the harsh environment. The accelerated aging test is conducted to simulate the effects of aging on the EM absorption coatings in a short period, including salt spray test, ultraviolet (UV) irradiation test, etc. However, even if the EM absorption coating has passed these accelerated aging tests individually, it may still deteriorate due to the combined effort of multiple aging factors. New methods and instruments are needed for the accelerated aging test with multiple aging factors. Xia et al. developed an instrument (Figure 20) to simulate the combined aging factors of UV irradiation and salt spray in the marine environment [83]. In the combined test of UV

irradiation and salt spray, the coating exhibited a faster deterioration in its EM absorption properties than in alternative tests of UV irradiation and salt spray.

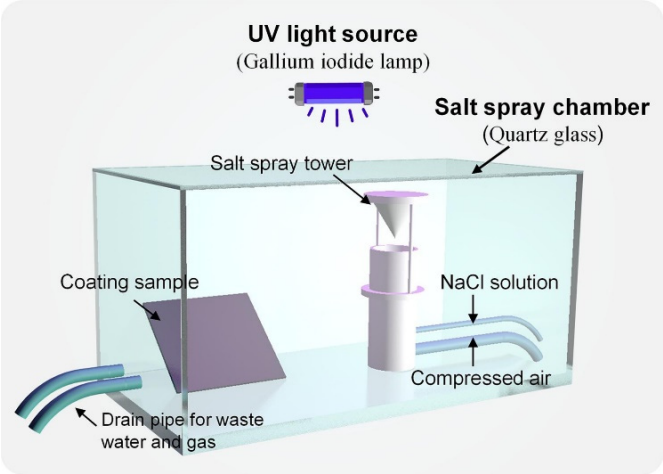

Figure 20. The instrument for the combined test of UV irradiation and salt spray [83]. Reprinted with permission from [83].

6. Application of EM Absorption Coatings

EM absorption coatings have numerous applications across various frequency ranges. The absorption performance of different kinds of EM absorption coatings is listed in Table 3. The choice of coating material depends on the specific operating frequency range and the desired functionality.

Table 3. The absorption performance of different kinds of EM coatings.

Kind of EM Absorption Coatings	EM Absorber	Maxtrix	RL_{min}			Reference
			dB	GHz *	Mm **	
Ceramic coatings	$LaFe_{12}O_{19}$	MgO/Al_2O_3	−39.30	4.4	4.5	[66]
	$Ba_4Fe_{2.6}Dy_{1.4}Nb_8O_{30}$	oxidized FeSiAl alloy	−48.20	4.0	3.5	[71]
	Fe_2AlB_2	/	−47.39	15.2	1.2	[84]
Polymeric coatings	Fe_3O_4/PANI	epoxy resin	−34.28	11.2	2	[85]
	CNF@Ni-C	epoxy resin	−49.77	13.44	2.2	[86]
	carbonyl iron/graphene	PU	−30.1	15.6	1	[43]
Metamaterial coatings	gyroid structured carbon-based material	/	−40	31	15	[56]
	TPMS-Shellular structured SiOC ceramics	/	−72.38	10.34	3.57	[57]

* This is the frequency at which the coating reaches its RL_{min}. ** This is the thickness at which the coating reaches its RL_{min}.

6.1. Broadband Absorption Coatings for Anti-Radar Stealth

Aircraft conducting covert operations have an urgent need for stealth coatings. In order to be undetectable by surveillance radar, the RCS of the aircraft needs to be smaller than 1 m^2 [87]. The RCS method utilizes a metal plate with EM absorption coatings to measure the reflected power of EM waves which pass through both surfaces. RCS indicates the area of the aircraft which reflects EM waves to the radar and can be calculated by Equation (15) [87,88].

$$RCS = 4\pi r^2 \frac{S_r}{S_t} \quad (15)$$

To achieve anti-radar stealth, coatings with EM strong absorption properties can be applied to reduce the RCS of the aircraft (Figure 21) [56]. Broadband absorption coatings

are in high demand due to the rapid advancements in radar technology across a wide range of frequency, including visual, infrared and microwave [89].

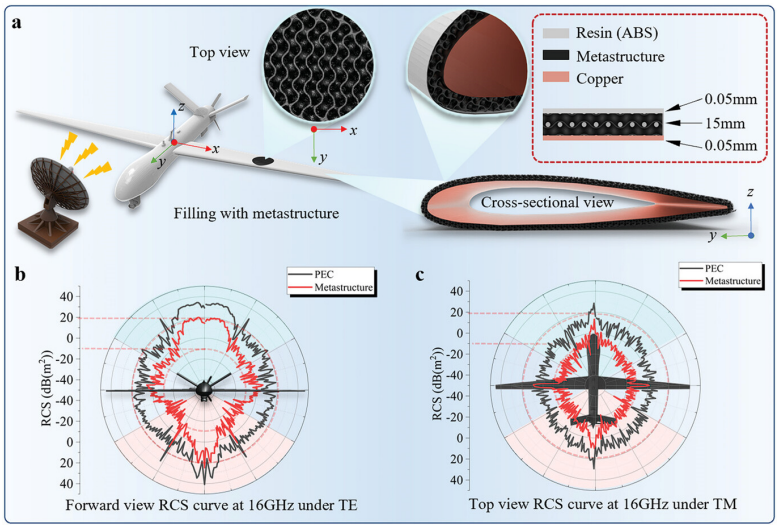

Figure 21. An example of the aircraft stealth coating and its RCS. (**a**) Drone with EM absorption coatings; (**b**) forward view RCS curve of the drone at 16 GHz under transverse electric (TE) polarization, and (**c**) top view RCS curve under transverse magnetic (TM) polarization. Reprinted with permission from [56].

6.2. Millimeter-Wave Absorption Coatings for 5G

The fifth generation commination technology (5G) has brought revolutionary impact to our life. 5G offers advantages of lower latency and higher bandwidth. High bandwidth requirement necessitates the inclusion of more antennas within mobile devices. It can potentially lead to EM interference between the packaged antennas [90]. The 5G RF system works in the GHz-THz range, with the wavelength in the order of millimeters. Therefore, millimeter wave absorption coatings are in urgent need for isolation EM signals between antennas. Materials such as graphene and MXene are of high conductivity and millimeter wave absorption properties. They are ideal coatings for 5G antennas [90,91].

6.3. Decametric-Wave Absorption Coatings for EM Shielding Suit

EM shielding suit is designed to protect the pregnant from EM radiation. The human body can be considered as a dielectric medium, and the decametric EM wave, whose wavelength is at the order of GHz, is absorbed to the greatest extent [92]. Therefore, decametric-wave absorption coatings are ideal for EM shielding suit. The suit used to be prepared by fabric blended with silver thread [93]. However, silver thread was expensive and the prepared suit was of limited commercial value. A low-cost and facile way to manufacture an EM shielding suit is liquid processing coating method, such as electroless deposition method. The fabric is immersed in a solution with metal precursors whdeposit-sits after reduction (Figure 22) [94]. Many efforts have been made in this field [95–97], but the durability of the EM shielding suit remains a problem.

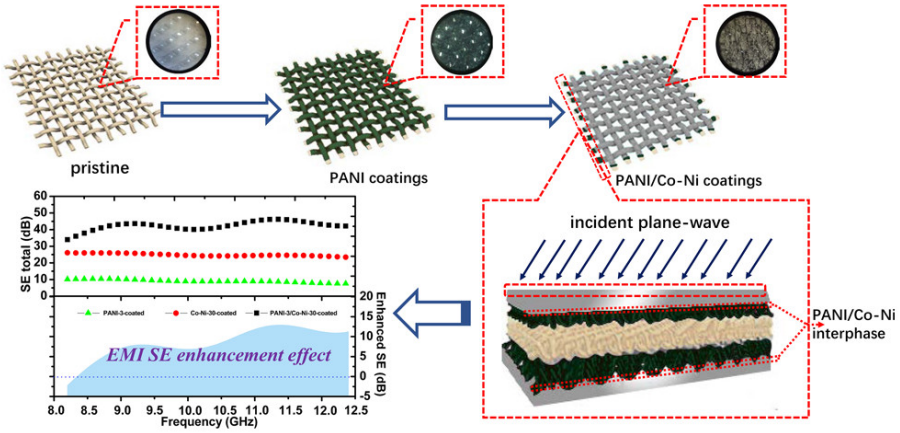

Figure 22. The preparation of EM shielding suit by electroless deposition. Reprinted with permission from [94].

7. Conclusions and Outlook

Recently progress has been made in the development of EM absorption coatings, especially in EM absorbers. These novel materials are promising feedstocks of absorption coatings, such as metallic nanomaterials, MXenes and MOF. However, to develop EM absorption coatings with thin, light, broadband and anti-aging properties, several problems remain to be solved.

Firstly, EM absorption mechanisms must be clarified. The mechanisms of EM absorption are not always practical in the design of EM absorption coatings, because they are qualitative and are from macroscopic aspects. Magnetic and dielectric dissipation have been used altogether to explain the EM absorption performance of the coating, but the dominant absorption mechanism is unclear. Some absorption mechanisms such as the eddy current loss are difficult to characterize. These mechanisms are impractical in designing EM absorption coatings. The problem may be solved by a quantitative study of absorption mechanisms from the molecular scale. Secondly, the overall performance of EM absorption coatings should be optimized. In extreme conditions, EM absorbers may undergo rapid aging and lose their absorbing properties. The EM absorption coatings must be improved in their anticorrosion properties and heat resistant properties to meet the practical need. Finally, scientists and engineers must make joint efforts for the manufacturing of novel EM absorption coatings. The processibility of coatings needs to be improved, including the rheological properties, thermostability, etc. Besides, manufacturing techniques need to be developed to produce high-performance EM absorption coatings on an industrial scale.

Author Contributions: Conceptualization, Y.J.; writing—original draft, Y.J.; writing—review and editing, Y.J., H.Y., Y.W., L.W. and B.N.; supervision, H.Y., L.W. and B.N. All authors have read and agreed to the published version of the manuscript.

Funding: This research received no external funding.

Institutional Review Board Statement: Not applicable.

Informed Consent Statement: Not applicable.

Data Availability Statement: Not applicable.

Acknowledgments: We thank Win Topatana for his help in language modification.

Conflicts of Interest: Author Yun Wang was employed by the company Zhejiang Tuanyuan Composite Materials Co., Ltd. Author Bohua Nan was employed by the company Shanghai Aerospace Equipments Manufacturer Co., Ltd. The remaining authors declare that the research was conducted in the absence of any commercial or financial relationships that could be construed as a potential conflict of interest.

References

1. Zhao, Y.; Ji, G. Multi-Spectrum Bands Compatibility: New Trends in Stealth Materials Research. *Sci. China Mater.* **2022**, *65*, 2936–2941. [CrossRef]
2. Pattanaik, B.; Chauhan, A. A Study of Stealth Technology. *Mater. Today Proc.* **2023**, *81*, 543–546. [CrossRef]
3. Liu, T.-T.; Fang, Y.-S.; Zhu, Y.-H.; Cao, M.-S. Green Building Materials Lit up by Electromagnetic Absorption Function: A Review. *J. Mater. Sci. Technol.* **2022**, *112*, 329–344. [CrossRef]
4. Xie, S.; Ji, Z.; Zhu, L.; Zhang, J.; Cao, Y.; Chen, J.; Liu, R.; Wang, J. Recent Progress in Electromagnetic Wave Absorption Building Materials. *J. Build. Eng.* **2020**, *27*, 100963. [CrossRef]
5. Lin, E.C. Radiation Risk from Medical Imaging. *Mayo Clin. Proc.* **2010**, *85*, 1142–1146. [CrossRef]
6. Frank, J.W. Electromagnetic Fields, 5G and Health: What about the Precautionary Principle? *J. Epidemiol. Community Health* **2021**, *75*, 562–566. [CrossRef]
7. Zhu, Y.; Mao, B.; Kato, N. IRS-aided High-Accuracy Positioning for Autonomous Driving Towards 6G: A Tutorial. *IEEE Veh. Technol. Mag.* **2024**, *19*, 85–92. [CrossRef]
8. Cheng, J.; Li, C.; Xiong, Y.; Zhang, H.; Raza, H.; Ullah, S.; Wu, J.; Zheng, G.; Cao, Q.; Zhang, D.; et al. Recent Advances in Design Strategies and Multifunctionality of Flexible Electromagnetic Interference Shielding Materials. *Nanomicro. Lett.* **2022**, *14*, 80. [CrossRef]
9. Liang, C.; Qiu, H.; Zhang, Y.; Liu, Y.; Gu, J. External Field-Assisted Techniques for Polymer Matrix Composites with Electromagnetic Interference Shielding. *Sci. Bull.* **2023**, *68*, 1938–1953. [CrossRef] [PubMed]
10. Tian, K.; Hu, D.; Wei, Q.; Fu, Q.; Deng, H. Recent Progress on Multifunctional Electromagnetic Interference Shielding Polymer Composites. *J. Mater. Sci. Technol.* **2023**, *134*, 106–131. [CrossRef]
11. Ghazanfarpour, M.; Kashani, Z.A.; Pakzad, R.; Abdi, F.; Rahnemaei, F.A.; Akbari, P.A.; Roozbeh, N. Effect of Electromagnetic Field on Abortion: A Systematic Review and Meta-Analysis. *Open Med.* **2021**, *16*, 1628–1641. [CrossRef] [PubMed]
12. Thaker, J.P.; Patel, M.B.; Jongnarangsin, K.; Liepa, V.V.; Thakur, R.K. Electromagnetic Interference with Pacemakers Caused by Portable Media Players. *Heart Rhythm.* **2008**, *5*, 538–544. [CrossRef]
13. Upadhyay, S.; Upadhya, A.; Salehi, W.; Gupta, G. The Medical Aspects of EMI Effect on Patients Implanted with Pacemakers. *Mater. Today Proc.* **2021**, *45*, 5243–5248. [CrossRef]
14. Wang, Y.; Pan, M.; Liang, X.; Li, B.; Zhang, S. Electromagnetic Wave Absorption Coating Material with Self-Healing Properties. *Macromol. Rapid Commun.* **2017**, *38*, 170047. [CrossRef] [PubMed]
15. Ganguly, S.; Kanovsky, N.; Das, P.; Gedanken, A.; Margel, S. Photopolymerized Thin Coating of Polypyrrole/Graphene Nanofiber/Iron Oxide onto Nonpolar Plastic for Flexible Electromagnetic Radiation Shielding, Strain Sensing, and Non-Contact Heating Applications. *Adv. Mater. Interfaces* **2021**, *8*, 2101255. [CrossRef]
16. Wang, X.; Lei, Z.; Ma, X.; He, G.; Xu, T.; Tan, J.; Wang, L.; Zhang, X.; Qu, L.; Zhang, X. A Lightweight MXene-Coated Nonwoven Fabric with Excellent Flame Retardancy, EMI Shielding, and Electrothermal/Photothermal Conversion for Wearable Heater. *Chem. Eng. J.* **2022**, *430*, 132605. [CrossRef]
17. de Lustrac, A.; Ratni, B.; Piau, G.-P.; Duval, Y.; Burokur, S.N. Tri-State Metasurface-Based Electromagnetic Screen with Switchable Reflection, Transmission, and Absorption Functionalities. *ACS Appl. Electron. Mater.* **2021**, *3*, 1184–1190. [CrossRef]
18. Wei, L.; Ma, J.; Ma, L.; Zhao, C.; Xu, M.; Qi, Q.; Zhang, W.; Zhang, L.; He, X.; Park, C.B. Computational Optimizing the Electromagnetic Wave Reflectivity of Double-Layered Polymer Nanocomposites. *Small Methods* **2022**, *6*, 2101510. [CrossRef]
19. Dobák, S.; Beatrice, C.; Tsakaloudi, V.; Fiorillo, F. Magnetic Losses in Soft Ferrites. *Magnetochemistry* **2022**, *8*, 60. [CrossRef]
20. Quan, B.; Liang, X.; Ji, G.; Cheng, Y.; Liu, W.; Ma, J.; Zhang, Y.; Li, D.; Xu, G. Dielectric Polarization in Electromagnetic Wave Absorption: Review and Perspective. *J. Alloys Compd.* **2017**, *728*, 1065–1075. [CrossRef]
21. Panahi-Sarmad, M.; Samsami, S.; Ghaffarkhah, A.; Hashemi, S.A.; Ghasemi, S.; Amini, M.; Wuttke, S.; Rojas, O.; Tam, K.C.; Jiang, F.; et al. MOF-Based Electromagnetic Shields Multiscale Design: Nanoscale Chemistry, Microscale Assembly, and Macroscale Manufacturing. *Adv. Funct. Mater.* **2024**, *34*, 2304473. [CrossRef]
22. Mohammed, I.; Mohammed, J.; Srivastava, A.K. Recent Progress in Hexagonal Ferrites Based Composites for Microwave Absorption. *Cryst. Res. Technol.* **2023**, *58*, 2200200. [CrossRef]
23. Xia, Y.; Gao, W.; Gao, C. A Review on Graphene-Based Electromagnetic Functional Materials: Electromagnetic Wave Shielding and Absorption. *Adv. Funct. Mater.* **2022**, *32*, 2204591. [CrossRef]
24. Jiang, X.; Zhang, L.; Yin, L.; Yang, G.; Xie, J.; Zhang, L.; Lu, H.; Liang, D.; Deng, L. Corrosion Behavior of Fluorinated Carbonyl Iron-Hydrophobic Composites in Neutral Salt Spray Environment. *Corros. Sci.* **2023**, *210*, 110823. [CrossRef]
25. Yuan, H.; Li, B.; Zhu, C.; Xie, Y.; Jiang, Y.; Chen, Y. Dielectric Behavior of Single Iron Atoms Dispersed on Nitrogen-Doped Nanocarbon. *Appl. Phys. Lett.* **2020**, *116*, 153101. [CrossRef]
26. Liu, H.; Li, X.; Zhao, X.; Zhang, M.; Liu, X.; Yang, S.; Wu, H.; Ma, Z. Large Annular Dipoles Bounded between Single-Atom Co and Co Cluster for Clarifying Electromagnetic Wave Absorbing Mechanism. *Adv. Funct. Mater.* **2023**, *33*, 2304442. [CrossRef]
27. Liang, H.; Chen, G.; Liu, D.; Li, Z.; Hui, S.; Yun, J.; Zhang, L.; Wu, H. Exploring the Ni 3*d* Orbital Unpaired Electrons Induced Polarization Loss Based on Ni Single-Atoms Model Absorber. *Adv. Funct. Mater.* **2023**, *33*, 2212604. [CrossRef]
28. Ma, C.; Ma, W.; Wang, T.; Ma, F.; Xu, X.; Feng, C.; Wang, W. An MXene Coating with Electromagnetic Wave Absorbing Performance. *Inorg. Chem. Commun.* **2023**, *151*, 110565. [CrossRef]

29. Verma, R.; Thakur, P.; Chauhan, A.; Jasrotia, R.; Thakur, A. A Review on MXene and Its' Composites for Electromagnetic Interference (EMI) Shielding Applications. *Carbon* **2023**, *208*, 170–190. [CrossRef]
30. Han, M.; Gogotsi, Y. Perspectives for Electromagnetic Radiation Protection with MXenes. *Carbon* **2023**, *204*, 17–25. [CrossRef]
31. Zhao, Y.; Hao, L.; Zhang, X.; Tan, S.; Li, H.; Zheng, J.; Ji, G. A Novel Strategy in Electromagnetic Wave Absorbing and Shielding Materials Design: Multi-Responsive Field Effect. *Small Sci.* **2022**, *2*, 2100077. [CrossRef]
32. Si, W.; Liao, Q.; Hou, W.; Chen, L.; Li, X.; Zhang, Z.; Sun, M.; Song, Y.; Qin, L. Low-Frequency Broadband Absorbing Coatings Based on MOFs: Design, Fabrication, Microstructure and Properties. *Coatings* **2022**, *12*, 766. [CrossRef]
33. Faisal, N.H.; Ahmed, R.; Sellami, N.; Prathuru, A.; Njuguna, J.; Venturi, F.; Hussain, T.; Nezhad, H.Y.; Katiyar, N.K.; Goel, S.; et al. Thermal Spray Coatings for Electromagnetic Wave Absorption and Interference Shielding: A Review and Future Challenges. *Adv. Eng. Mater.* **2022**, *24*, 2200171. [CrossRef]
34. Deng, Z.; Jiang, P.; Wang, Z.; Xu, L.; Yu, Z.; Zhang, H. Scalable Production of Catecholamine-Densified MXene Coatings for Electromagnetic Shielding and Infrared Stealth. *Small* **2023**, *19*, 2304278. [CrossRef]
35. Xie, Y.; Liu, S.; Huang, K.; Chen, B.; Shi, P.; Chen, Z.; Liu, B.; Liu, K.; Wu, Z.; Chen, K.; et al. Ultra-Broadband Strong Electromagnetic Interference Shielding with Ferromagnetic Graphene Quartz Fabric. *Adv. Mater.* **2022**, *34*, 2202982. [CrossRef]
36. Wang, T.; Chen, G.; Zhu, J.; Gong, H.; Zhang, L.; Wu, H. Deep Understanding of Impedance Matching and Quarter Wavelength Theory in Electromagnetic Wave Absorption. *J. Colloid Interface Sci.* **2021**, *595*, 1–5. [CrossRef] [PubMed]
37. Huo, J.; Wang, L.; Yu, H. Polymeric Nanocomposites for Electromagnetic Wave Absorption. *J. Mater. Sci.* **2009**, *44*, 3917–3927. [CrossRef]
38. Wei, H.; Zhang, Z.; Hussain, G.; Zhou, L.; Li, Q.; Ostrikov, K. Techniques to Enhance Magnetic Permeability in Microwave Absorbing Materials. *Appl. Mater. Today* **2020**, *19*, 100596. [CrossRef]
39. Zhou, Y.; Wang, S.-J.; Li, D.-S.; Jiang, L. Lightweight and Recoverable ANF/RGO/PI Composite Aerogels for Broad and High-Performance Microwave Absorption. *Compos. B Eng.* **2021**, *213*, 108701. [CrossRef]
40. Qin, M.; Zhang, L.; Wu, H. Dielectric Loss Mechanism in Electromagnetic Wave Absorbing Materials. *Adv. Sci.* **2022**, *9*, 2105553. [CrossRef]
41. Zhang, J.; Ma, M.; Bi, Y.; Liao, Z.; Ma, Y.; Huang, W.; Lyu, P.; Feng, C. A Review of Epoxy-Based Composite Materials: Synthesis, Structure and Application for Electromagnetic Wave Absorption. *J. Alloys Compd.* **2022**, *922*, 166096. [CrossRef]
42. Lee, S.H.; Kim, J.Y.; Koo, C.M.; Kim, W.N. Effects of Processing Methods on the Electrical Conductivity, Electromagnetic Parameters, and EMI Shielding Effectiveness of Polypropylene/Nickel-Coated Carbon Fiber Composites. *Macromol. Res.* **2017**, *25*, 936–943. [CrossRef]
43. Duan, Y.; Liu, Y.; Cui, Y.; Ma, G.; Tongmin, W. Graphene to Tune Microwave Absorption Frequencies and Enhance Absorption Properties of Carbonyl Iron/Polyurethane Coating. *Prog. Org. Coat.* **2018**, *125*, 89–98. [CrossRef]
44. Zhao, W.; Zhang, Q.; Zhang, H.; Zhang, J. Preparation of PS/Ag Microspheres and Its Application in Microwave Absorbing Coating. *J. Alloys Compd.* **2009**, *473*, 206–211. [CrossRef]
45. Fu, Z.; Pang, A.; Luo, H.; Zhou, K.; Yang, H. Research Progress of Ceramic Matrix Composites for High Temperature Stealth Technology Based on Multi-Scale Collaborative Design. *J. Mater. Res. Technol.* **2022**, *18*, 2770–2783. [CrossRef]
46. Wu, C.; Wang, J.; Zhang, X.; Kang, L.; Cao, X.; Zhang, Y.; Niu, Y.; Yu, Y.; Fu, H.; Shen, Z.; et al. Hollow Gradient-Structured Iron-Anchored Carbon Nanospheres for Enhanced Electromagnetic Wave Absorption. *Nanomicro Lett.* **2023**, *15*, 7. [CrossRef] [PubMed]
47. Zhang, X.; Tian, X.; Qiao, J.; Fang, X.; Liu, K.; Liu, C.; Lin, J.; Li, L.; Liu, W.; Liu, J.; et al. In-Situ Fabrication of Sustainable-N-Doped-Carbon-Nanotube-Encapsulated CoNi Heterogenous Nanocomposites for High-Efficiency Electromagnetic Wave Absorption. *Small* **2023**, *19*, 2302686. [CrossRef] [PubMed]
48. Liu, Y.; Wang, S.; Wang, Q.; Su, X. Electromagnetic and Microwave Absorption Properties of Flexible Fabric Coatings Containing Ag Decorated Spherical Graphene Powders with FSS Incorporation. *Ceram. Int.* **2024**, *50*, 11075–11084. [CrossRef]
49. Yu, M.; Huang, Y.; Liu, X.; Zhao, X.; Fan, W.; She, K. In Situ Modification of MXene Nanosheets with Polyaniline Nanorods for Lightweight and Broadband Electromagnetic Wave Absorption. *Carbon* **2023**, *208*, 311–321. [CrossRef]
50. Zheng, C.; Ning, M.; Zou, Z.; Lv, G.; Wu, Q.; Hou, J.; Man, Q.; Li, R. Two Birds with One Stone: Broadband Electromagnetic Wave Absorption and Anticorrosion Performance in 2–18GHz for Prussian Blue Analog Derivatives Aimed for Practical Applications. *Small* **2023**, *19*, 2208211. [CrossRef]
51. Xie, T.; Li, S.; Ma, L.; Li, J.; Pang, S.; Hu, C.; Zhao, R.; Tang, S. Bimetallic MOF-Derived Composites with Broad Electromagnetic Wave Absorption and Strong Corrosion Resistance. *Carbon* **2023**, *208*, 33–42. [CrossRef]
52. Zhang, X.; Tian, X.-L.; Qin, Y.; Qiao, J.; Pan, F.; Wu, N.; Wang, C.; Zhao, S.; Liu, W.; Cui, J.; et al. Conductive Metal–Organic Frameworks with Tunable Dielectric Properties for Boosting Electromagnetic Wave Absorption. *ACS Nano* **2023**, *17*, 12510–12518. [CrossRef]
53. Liu, J.; Liang, H.; Wei, B.; Yun, J.; Zhang, L.; Wu, H. "Matryoshka Doll" Heterostructures Induce Electromagnetic Parameters Fluctuation to Tailor Electromagnetic Wave Absorption. *Small Struct.* **2023**, *4*, 2200379. [CrossRef]
54. Li, G.; Ma, S.; Li, Z.; Zhang, Y.; Cao, Y.; Huang, Y. Temperature-Induced Self-Decomposition Doping of Fe_3GeTe_2 to Achieve Ultra-High Tc of 496K for Multispectral Compatible Strong Electromagnetic Wave Absorption. *Adv. Funct. Mater.* **2023**, *33*, 2210578. [CrossRef]

55. Xia, W.; Li, C.; Zhang, S.; Wang, X.; Wang, S.; Yang, Q.; Li, W.; Xiong, C.; Huang, J.; Wang, Q. Ho-Ion-Polymer/Graphene Heterojunctions Toward Room-Temperature Ferromagnets. *Small* **2023**, *19*, 2300385. [CrossRef]
56. An, Q.; Li, D.; Liao, W.; Liu, T.; Joralmon, D.; Li, X.; Zhao, J. A Novel Ultra-Wideband Electromagnetic-Wave-Absorbing Metastructure Inspired by Bionic Gyroid Structures. *Adv. Mater.* **2023**, *35*, 2300659. [CrossRef]
57. Yao, L.; Yang, W.; Zhou, S.; Mei, H.; Li, Y.; Dassios, K.G.; Riedel, R.; Liu, C.; Cheng, L.; Zhang, L. Top-down Parametrization-Design of Orientation-Reinforced SiOC-Based Perfect Metamaterial Microwave Absorber with Wide-Temperature Adaptability. *Acta Mater.* **2023**, *249*, 118803. [CrossRef]
58. Tao, J.; Zhou, J.; Yao, Z.; Jiao, Z.; Wei, B.; Tan, R.; Li, Z. Multi-Shell Hollow Porous Carbon Nanoparticles with Excellent Microwave Absorption Properties. *Carbon* **2021**, *172*, 542–555. [CrossRef]
59. Zhang, F.; Jia, Z.; Zhou, J.; Liu, J.; Wu, G.; Yin, P. Metal-Organic Framework-Derived Carbon Nanotubes for Broadband Electromagnetic Wave Absorption. *Chem. Eng. J.* **2022**, *450*, 138205. [CrossRef]
60. Liu, J.; Zhang, L.; Wu, H. Electromagnetic Wave-Absorbing Performance of Carbons, Carbides, Oxides, Ferrites and Sulfides: Review and Perspective. *J. Phys. D Appl. Phys.* **2021**, *54*, 203001. [CrossRef]
61. Anasori, B.; Naguib, M. Two-Dimensional MXenes. *MRS Bull.* **2023**, *48*, 238–244. [CrossRef]
62. Dai, B.; Ma, Y.; Dong, F.; Yu, J.; Ma, M.; Thabet, H.K.; El-Bahy, S.M.; Ibrahim, M.M.; Huang, M.; Seok, I.; et al. Overview of MXene and Conducting Polymer Matrix Composites for Electromagnetic Wave Absorption. *Adv. Compos. Hybrid. Mater.* **2022**, *5*, 704–754. [CrossRef]
63. Fan, B.; Li, N.; Dai, B.; Shang, S.; Guan, L.; Zhao, B.; Wang, X.; Bai, Z.; Zhang, R. Investigation of Adjacent Spacing Dependent Microwave Absorption Properties of Lamellar Structural $Ti_3C_2T_x$ MXenes. *Adv. Powder Technol.* **2020**, *31*, 808–815. [CrossRef]
64. Zhou, X.; Li, S.; Zhang, M.; Yuan, X.; Wen, J.; Xi, H.; Wu, H.; Ma, X. MXene/PEO Aerogels with Two-Hierarchically Porous Architecture for Electromagnetic Wave Absorption. *Carbon* **2023**, *204*, 538–546. [CrossRef]
65. Zhang, Y.; Ruan, K.; Zhou, K.; Gu, J. Controlled Distributed $Ti_3C_2T_x$ Hollow Microspheres on Thermally Conductive Polyimide Composite Films for Excellent Electromagnetic Interference Shielding. *Adv. Mater.* **2023**, *35*, 2211642. [CrossRef] [PubMed]
66. Niu, X.; Huang, P.; Wang, Y.; Zou, B. Preparation and Characterization of a Composite Ceramic Coating Containing Absorber $LaFe_{12}O_{19}$ by Plasma Spraying. *Ceram. Int.* **2023**, *49*, 27079–27085. [CrossRef]
67. Ren, S.; Yu, H.; Wang, L.; Huang, Z.; Lin, T.; Huang, Y.; Yang, J.; Hong, Y.; Liu, J. State of the Art and Prospects in Metal-Organic Framework-Derived Microwave Absorption Materials. *Nanomicro. Lett.* **2022**, *14*, 68. [CrossRef] [PubMed]
68. Hossain, M.D.; Hossain, M.A.; Sikder, S.S. Hysteresis Loop Properties of Rare Earth Doped Spinel Ferrites: A Review. *J. Magn. Magn. Mater.* **2022**, *564*, 170095. [CrossRef]
69. Liu, Y.; Li, C.; Fang, B.; Chen, L.; Xu, J.; Liu, F.; Xu, L.; Li, X.; Tang, Y.; Hong, Z.; et al. Research Progress in Tunable Metamaterial Absorbers. *Adv. Photonics Res.* **2024**, *5*, 2300258. [CrossRef]
70. Yao, H.; Qing, Y.; Li, Y.; Wen, J.; Li, W.; Cao, Y.; Luo, F. Effect of B_4C Content and Annealing on Complex Permittivity and Microwave-Absorption Properties of B_4C/Al_2O_3 Coatings. *J. Eur. Ceram. Soc.* **2023**, *43*, 1450–1458. [CrossRef]
71. Huang, P.; Niu, X.; Wang, Y.; Zou, B. Ultra-broadband Electromagnetic Wave Absorption of Ceramic Composite Coating by Atmospheric Plasma Spraying. *J. Am. Ceram. Soc.* **2023**, *106*, 5832–5845. [CrossRef]
72. Deng, Z.; Li, L.; Tang, P.; Jiao, C.; Yu, Z.-Z.; Koo, C.M.; Zhang, H.-B. Controllable Surface-Grafted MXene Inks for Electromagnetic Wave Modulation and Infrared Anti-Counterfeiting Applications. *ACS Nano* **2022**, *16*, 16976–16986. [CrossRef]
73. Ma, Z.; Xiang, X.; Shao, L.; Zhang, Y.; Gu, J. Multifunctional Wearable Silver Nanowire Decorated Leather Nanocomposites for Joule Heating, Electromagnetic Interference Shielding and Piezoresistive Sensing. *Angew. Chem. Int. Ed.* **2022**, *61*, e202200705. [CrossRef]
74. Wang, Y.; Li, J.; Li, W.; Ma, L.; Lin, J.; Ye, S.; Zhao, Q.; Liu, Y.; Zhao, S. Flexible Polypyrrole-Coated Polyamide Based Mats for Broadband Microwave Absorption and Electromagnetic Interference Shielding with Low Reflection. *ACS Appl. Polym. Mater.* **2023**, *5*, 2995–3004. [CrossRef]
75. Wang, B.; Fu, Y.; Li, J.; Wu, Q.; Wang, X.; Liu, T. Construction of Co@C Nanocapsules by One-Step Carbon Reduction of Single-Crystal Co3O4 Nanoparticles: Ultra-Wideband Microwave Absorber Verified via Coaxial and Arch Methods. *Chem. Eng. J.* **2022**, *445*, 136863. [CrossRef]
76. Wu, C.; Bi, K.; Yan, M. Scalable Self-Supported $FeNi_3/Mo_2C$ Flexible Paper for Enhanced Electromagnetic Wave Absorption Evaluated via Coaxial, Waveguide and Arch Methods. *J. Mater. Chem. C Mater.* **2020**, *8*, 10204–10212. [CrossRef]
77. Peng, M.; Qin, F. Clarification of Basic Concepts for Electromagnetic Interference Shielding Effectiveness. *J. Appl. Phys.* **2021**, *130*, 225108. [CrossRef]
78. Costa, F.; Borgese, M.; Degiorgi, M.; Monorchio, A. Electromagnetic Characterisation of Materials by Using Transmission/Reflection (T/R) Devices. *Electronics* **2017**, *6*, 95. [CrossRef]
79. Guo, Y.; Ruan, K.; Wang, G.; Gu, J. Advances and Mechanisms in Polymer Composites toward Thermal Conduction and Electromagnetic Wave Absorption. *Sci. Bull.* **2023**, *68*, 1195–1212. [CrossRef] [PubMed]
80. Yang, Y.; Logesh, K.; Mehrez, S.; Huynen, I.; Elbadawy, I.; Mohanavel, V.; Alamri, S. Rational Construction of Wideband Electromagnetic Wave Absorber Using Hybrid $FeWO_4$-Based Nanocomposite Structures and Tested by the Free-Space Method. *Ceram. Int.* **2023**, *49*, 2130–2139. [CrossRef]
81. Samadpour, E.; Kiani, E.; Hosein Shams, M. Microwave Permeability and Electromagnetic Wave Absorption Properties of Co_2Y Nanocomposites. *Mater. Sci. Eng. B* **2023**, *298*, 116825. [CrossRef]

82. Shao, N.; Li, J.; Che, S.; Zheng, J.; Qiao, L.; Ying, Y.; Yu, J.; Li, W. L and S Band Microwave Absorption Properties of Z-Type Hexaferrite $Ba_3Co_2Fe_{24}O_{41}$ Synthesized at Low Temperature. *J. Alloys Compd.* **2023**, *968*, 171926. [CrossRef]
83. Xia, L.; Wang, K.; Xu, W.; Kong, M.; Huang, Y.; Lv, Y.; Li, G. Synergistic Acceleration Effects of Ultraviolet and Salt Spray on the Degradation and Failure of Electromagnetic Wave-Absorbing Coatings. *Prog. Org. Coat.* **2023**, *182*, 107686. [CrossRef]
84. Zhi, Q.; Wu, C.; Li, M.; Liu, J.; Zhang, R.; Min, Z.; Chen, Y.; Li, H.; Fan, B. Fe_2AlB_2: A Novel Ferromagnetic Material with Superior Electromagnetic Wave Absorption Performance. *Ceram. Int.* **2023**, *49*, 34182–34190. [CrossRef]
85. Talebi, H.; Olad, A.; Nosrati, R. Fe_3O_4/PANI Nanocomposite Core-Shell Structure in Epoxy Resin Matrix for the Application as Electromagnetic Waves Absorber. *Prog. Org. Coat.* **2022**, *163*, 106665. [CrossRef]
86. Qian, Y.; Tao, Y.; Li, W.; Li, Y.; Xu, T.; Hao, J.; Jiang, Q.; Luo, Y.; Yang, J. High Electromagnetic Wave Absorption and Thermal Management Performance in 3D CNF@C-Ni/Epoxy Resin Composites. *Chem. Eng. J.* **2021**, *425*, 131608. [CrossRef]
87. Neethu, L.S.; Sudhi, S. Low Frequency Radar for Improving Radar Cross Section. In Proceedings of the 2023 International Conference on Control, Thiruvananthapuram, India, 19–21 May 2023. [CrossRef]
88. Taj, Z.U.D.; Bilal, A.; Awais, M.; Salamat, S.; Abbas, M.; Maqsood, A. Design Exploration and Optimization of Aerodynamics and Radar Cross Section for a Fighter Aircraft. *Aerosp. Sci. Technol.* **2023**, *133*, 108114. [CrossRef]
89. Shirke, N.; Ghase, V.; Jamdar, V. Recent Advances in Stealth Coating. *Polym. Bull.* **2024**, *81*, 1–30. [CrossRef]
90. Song, R.; Mao, B.; Wang, Z.; Hui, Y.; Zhang, N.; Fang, R.; Zhang, J.; Wu, Y.; Ge, Q.; Novoselov, K.S.; et al. Comparison of Copper and Graphene-Assembled Films in 5G Wireless Communication and THz Electromagnetic-Interference Shielding. *Proc. Natl. Acad. Sci. USA* **2023**, *120*, e2209807120. [CrossRef]
91. Li, J.; Tsai, M.; Chiu, R.; He, E.; Hsieh, A.; Tsai, M.-F.; Chu, F.; Chen, J.Y.; Jian, S.; Chen, S.; et al. EMI Shielding Technology in 5G RF System in Package Module. In Proceedings of the 2020 IEEE 70th Electronic Components and Technology Conference (ECTC), Orlando, FL, USA, 5 August 2020. [CrossRef]
92. Pethig, R. Dielectric properties of body tissues. *Clin. Phys. Physiol. Meas* **1987**, *8*, 5–12. [CrossRef]
93. Malarić, K.; Šaravanja, B.; Pušić, T. Microwave Radiation Protective Suit with Silver Threads. In Proceedings of the 4th International Conference on Smart Grid Metrology (SMAGRIMET), Cavtat, Croatia, 24–28 April 2023. [CrossRef]
94. Zhao, H.; Hou, L.; Bi, S.; Lu, Y. Enhanced X-Band Electromagnetic-Interference Shielding Performance of Layer-Structured Fabric-Supported Polyaniline/Cobalt–Nickel Coatings. *ACS Appl. Mater. Interfaces* **2017**, *9*, 33059–33070. [CrossRef] [PubMed]
95. Liu, W.; Sun, D.; Ma, H.; Chen, Z.; Gui, C.; Huang, J. A Facile Process Combined with Electroless Deposition and Hydrophobic Treatment to Fabricate Self-Cleaning Radiation Protection Suits for Pregnant Woman. *Fibers Polym.* **2022**, *23*, 1309–1317. [CrossRef]
96. Zhou, S.; Dong, J.; Li, X.; Zhao, X.; Zhang, Q. Continuous Surface Metallization of Polyimide Fibers for Textile-Substrate Electromagnetic Shielding Applications. *Adv. Fiber Mater.* **2023**, *5*, 1892–1904. [CrossRef]
97. Gui, C.; Sun, D.; Liu, W.; Ma, H.; Chen, Z.; Li, P.; Huang, J. Electroless Plating Process for the Manufacture of Radiation Protection Suits for Pregnant Woman: Effect of Bending on Its Electromagnetic Shielding Performance. *J. Ind. Text.* **2022**, *51*, 3176S–3187S. [CrossRef]